Robustness of heat transfer in confined inclined convection at high Prandtl number

Linfeng Jiang,[1] Chao Sun,[1,*] and Enrico Calzavarini[2,†]

[1]*Center for Combustion Energy, Key Laboratory for Thermal Science and Power Engineering of Ministry of Education,*
Department of Energy and Power Engineering, Tsinghua University, Beijing 100084, China
[2]*Université de Lille, Unité de Mécanique de Lille, UML EA 7512, F 59000 Lille, France*

We investigate the dependency of the magnitude of heat transfer in a convection cell as a function of its inclination by means of experiments and simulations. The study is performed with a working fluid of large Prandtl number, $\mathrm{Pr} \simeq 480$, and at Rayleigh numbers $\mathrm{Ra} \simeq 10^8$ and $\mathrm{Ra} \simeq 5 \times 10^8$ in a quasi-two-dimensional rectangular cell with unit aspect ratio. By changing the inclination angle (β) of the convection cell, the character of the flow can be changed from moderately turbulent, for $\beta = 0°$, to laminar and steady at $\beta = 90°$. The global heat transfer is found to be insensitive to the drastic reduction of turbulent intensity, with maximal relative variations of the order of 20% at $\mathrm{Ra} \simeq 10^8$ and 10% at $\mathrm{Ra} \simeq 5 \times 10^8$, while the Reynolds number, based on the global root-mean-square velocity, is strongly affected with a decay of more than 85% occurring in the laminar regime. We show that the intensity of the heat flux in the turbulent regime can be only weakly enhanced by establishing a large-scale circulation flow by means of small inclinations. However, in the laminar regime the heat is transported solely by a slow large-scale circulation flow which exhibits large correlations between the velocity and temperature fields. For inclination angles close to the transition regime in-between the turbulentlike and laminar state, a quasiperiodic heat-flow bursting phenomenon is observed.

I. INTRODUCTION

Natural thermal convection in enclosures filled with fluids has a pivotal role in a long list of engineering and geophysical systems. The fluid motion generated by heating a closed container from below and cooling it above, known as Rayleigh-Bénard convection (RBC), is a classical model system in fluid mechanics that has been studied over several decades [1–5]. Another frequently encountered natural thermal convection setting, termed vertical convection (VC) system, consists instead of a container heated and cooled from the lateral vertical sides, and it has been equally extensively studied [6–10]. The sole difference between RBC and VC systems is the different directions between the gravity field and the externally imposed temperature gradient, i.e., gravity is antiparallel to the temperature gradient in RBC while it is orthogonal to it in VC. This is responsible for the different stability properties of the two systems, while in the RBC a precise minimal (vertical) thermal gap is necessary for the onset of fluid motion, in the VC a flow always exists independently of the (horizontal) thermal gap. For a specific geometry, grossly described by the width over height aspect ratio, $\Gamma = L/H$, the internal flow of thermal convection in both such systems is determined by two control parameters, the Rayleigh number $\mathrm{Ra} = \alpha g \Delta T H^3 / \nu \kappa$ and the Prandtl number $\mathrm{Pr} = \nu/\kappa$. Here α refers to the volumetric thermal expansion coefficient, g the acceleration due to gravity, ΔT the temperature difference between hot and cold boundaries,

ν the kinematic viscosity and κ the thermal diffusivity of the fluid. Note that this is true only for small temperature gaps so that the material properties can be reasonably taken as constant, i.e., in Oberbeck-Boussinesq conditions [3]. One of the key response parameters of thermal convection is the Nusselt number, Nu, which provides the ratio of the global mean heat flux through the system over the purely conductive flux. Another key response is the global intensity of turbulence, which can be characterized by the Reynolds number, Re, in terms of a suitably defined characteristic velocity for the flow.

The dependence of the two response global parameters (Nu, Re) as functions of the control ones (Ra, Pr, Γ) exhibits different behaviors for RBC and VC. Experimental measurements and numerical simulations of the RBC system over wide parameter ranges have revealed many features of the heat transfer mechanisms, and a phenomenological theory capable to predict the functional dependence Nu(Ra, Pr) and Re(Ra, Pr) in the RBC system is nowadays available [11,12]. In RBC, the exponent of the power-law scaling of Nu on Ra is most of the time in the range between 1/4 and 1/3 [1,3,11,13] (it is expected to be larger only in the asymptotic Ra limit [3]). In the VC system the same scaling exponent is also found to vary in the same range [7,9,14–18] and attempts to frame this into a phenomenological theory have been put forward [10]. However, the VC and the RBC flows can be in different states for the same control parameters. For example, for $\mathrm{Ra} \sim \mathrm{O}(10^8)$, $\mathrm{Pr} \simeq 1$ and cylindrical container of aspect ratio 1, the VC flow is in laminar state, while the RBC flow is turbulent [19]. This has led to formulate the hypothesis that the presence of a turbulent flow might not be essential in determining the classical near to 1/3 power-law scaling of Nu as a function of Ra in such systems [7].

More recently an extension of the RBC and VC system has been studied which takes into account the effect of an arbitrary inclination angle (β) of the bottom wall of the system with respect to the horizontal, so that the limiting cases $\beta = 0°$ corresponds to RBC and $\beta = 90°$ to VC. Such a system, denoted as confined inclined convection (CIC) [19–21] has a larger space of control parameters, namely, Ra, Pr, Γ, β, and its key response functions Nu and Re appear to be more intricately dependent on the set of control parameters. There are presently few series of experimental studies which have explored CIC in the full $[0°, 90°]$ inclination angle interval. These have been performed either in a quasi-two-dimensional rectangular cell with $\Gamma_x = 1$, $\Gamma_z = 1/4$ with water, Pr $\simeq 6.3$ and Ra $\simeq 4.4 \times 10^9$ [22] and with silicon oil, Pr $\simeq 10$ and Ra $\simeq 6.8 \times 10^{10}$ [23], or in cylindrical cells $\Gamma = 1$ and $\Gamma = 1/20$ with liquid sodium, Pr $= 0.0094$, at, respectively, Ra $= 1.47 \times 10^7$ [24] and Ra $= 2.4 \times 10^6$ [25]. While the first studies (water and silicon-oil) revealed a weak monotonic decrease of the heat flux, with a maximal reduction of 20% with respect to the RBC value, the second group of studies displayed always an overall increment of Nu with the existence of an optimal inclination around $\beta \simeq 65°$–$70°$ for which the increment was 20% in the $\Gamma = 1$, and remarkably as high as 1100% in the $\Gamma = 1/20$ system. On the numerical side, a thorough series of studies in $\Gamma = 1$ cylindrical setting have been conducted for $0.1 \leqslant$ Pr $\leqslant 100$ and $10^6 \leqslant$ Ra $\leqslant 10^8$ [19]. This highlighted that the relative variation of Nu (with respect to the RBC case) is always moderate $<25\%$ for CIC system with $\Gamma = 1$. Furthermore, Nu(β) appears to be a nonmonotonic function characterized either by one or two local maxima [19]. A second series of numerical studies have been conducted at Pr $= 0.1$ and Ra ranging from 10^6 to 10^9 in a narrower cylindrical system ($\Gamma = 1/5$) which showed that Nu increases up to 120% with the inclination angle [20]. It is worth mentioning also the only detailed study that reports in parallel experimental and numerical results [26]. Such experiments were performed with air, Pr $\simeq 0.7$, at Ra $\leqslant 10^8$ in a rectangular cell $\Gamma_x = 0.75$ and $\Gamma_x = 1.5$ and reported too a weak decrease of the relative Nu with the tilting angle. From the above mentioned studies one can extract the following general trends: in unit aspect ratio cells the variation in the global heat-flux with Nu are moderate $<20\%$. Conversely, the variations are much bigger in elongated systems. The form of Nu(β) is highly variable (monotonically decreasing, increasing with one or more peaks) and appears to be more sensitive to Pr number rather than to Ra. It appears that the research on the CIC system is still in a taxonomical phase: The current studies indeed try to collect information to produce a more complete map of the phenomenology of such a complex system, which depends on at least four control parameters (if not more because inclined convection might indeed critically depend also on the cell shape, e.g., rectangular or cylindrical).

With this in mind, in this paper we consider the still unexplored case of very large Prandtl number inclined convection cell. More precisely, we focus on the dynamics of a quasi-two-dimensional rectangular cell, the same geometry as [22,23] in a fluid with Prandtl number [Pr $\simeq O(10^2)$] and at Rayleigh numbers [Ra $\simeq O(10^8)$] and as before we control the flow from the developed turbulent state to the laminar state by inclining the system with $\beta \in [0°, 90°]$. To complement
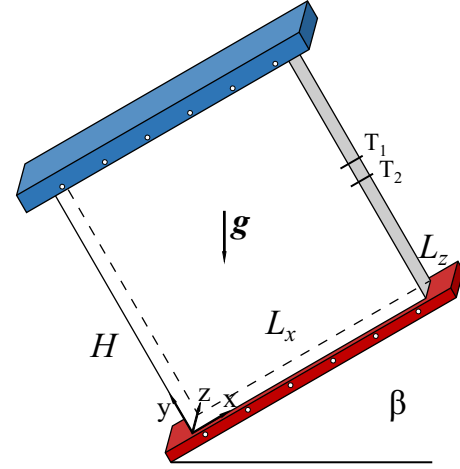

FIG. 1. A sketch of the rectangular convection cell and the coordinate frame adopted in this study. The height, length and width of the cell are denoted by H, L_x, and L_z, respectively. β is the inclination angle relative to the horizontal plane. The x and y coordinate axes align with the bottom plate and the sidewall respectively. Circles in the top bottom plates indicate the position of the 12 thermistors used to monitor the global thermal gap ΔT, while $T_{1,2}$ show the positions of the two thermal probes employed for the measurement of the intensity of the local flow.

the experiments and explain the observed trends, numerical simulations in very similar conditions are also carried out. We do not seek here to explore the scaling laws of the response parameters as a function of Ra or Pr but rather we focus on the amplitude variation of the global response parameters (together with their temporal fluctuations) as a function of the system inclination angle. Similar to the question raised in Ref. [7], we aim at understanding whether the presence of a turbulent flow is essential in determining the magnitude of heat transfer in such a system. It appears that, as seen in similar CIC experiments at $\Gamma = 1$ the system self-organize in such a way to robustly keep a stable average global heat flow magnitude, within 20%, independently of the inclination angle and so independently of the presence of turbulent fluctuations. The functional shape of the modulation of Nu with the inclination is instead peculiar of the studied system, and the behavior observed here can be in part attributed to the high flow-temperature coherence displayed by high-Pr fluid dynamics.

II. SETUPS AND METHODS

A. Experiments

The experimental setup employed in this study is sketched in Fig. 1. It is a rectangular cell, with height $H = 240$ mm, length $L_x = 240$ mm, and width $L_z = 60$ mm. The relative aspect ratios of the length and width with respect to height are therefore $\Gamma_x = L_x/H = 1$ and $\Gamma_z = L_z/H = 1/4$, respectively. The experiments presented here have been conducted by means of silicone oil as working fluid at a mean temperature $T_m = 25$ °C which corresponds to a Prandtl number Pr $\simeq 480$. The lateral walls of the cell are made by acrylic foils of 5 mm thickness and they are kept within two thick copper top

and bottom plates of 35 and 25 mm, respectively, supported by four steel pillars. The temperature of the top plate is kept constant by a refrigerated liquid circulating bath (Polyscience AD15R-40-A12Y) with a temperature stability of ± 0.01 K. While a film heater is embedded into the bottom plate and it is powered by a power supply to provide a constant heat flux. To decrease the systematic errors associated with possible heat losses, a thermostat box, with setting at ambient temperature at $25\,°C \pm 0.4\,°C$, is used to shield the full convection system. The temperatures of the plates are measured by means of six embedded thermistors per plate, whose electric resistances are measured by a digital multimeter (NI PXIe-4065) at a constant sampling rate of 3 Hz. The corresponding temperatures are calculated via the Steihart-Hart function [27]. The experiments are performed at two time-averaged temperature differences, $\Delta T = 4.0 \pm 0.1$ K (corresponding Ra $\simeq 10^8$) and $\Delta T = 20.0 \pm 0.1$ K (corresponding Ra $\simeq 5 \times 10^8$). With such temperature differences non-Oberbeck-Boussinesq effects in silicon oil are negligible.

The measurements of the Nusselt number in the experiments is based on the relation Nu $= QH/(\chi \Delta T)$, where Q is the time-averaged total heat-flux through the system and χ the thermal conductivity of the fluid. Here Q is calculated from the electric power used by the heater (P) via the relation $Q = P/(L_x\, L_z) = V^2/(R\, L_x\, L_z)$, where V is the voltage, R the electric resistance of the heater. The measurement of the Reynolds number, Re $= UH/\nu$, requires instead an estimate of a characteristic velocity amplitude of the flow, U. In the experiment we take for U the local fluid velocity in a position at half height in the cell and 1 cm away from the sidewall, as shown in Fig. 1. This is done by means of two thermistors (T_1 and T_2 in Fig. 1) of 0.2 mm in diameter and 1.5 cm apart. We use two Wheatstone bridges and lock-in amplifiers to measure the temperatures from such probes at a sampling rate of 128 Hz. At this sampling rate the cross-correlation from the thermistor time-series results to be smooth and the elliptic model [28] can be used to reconstruct the intensity of the velocity.

B. Numerical simulations

Next to the experiments we conduct direct numerical simulations (DNS) of thermal convection in an inclined cell at the same Pr and Ra numbers as in the experiments. We adopt, however, the simplifying assumption of (i) having a two-dimensional system ($\Gamma_x = 1$ and $\Gamma_z = 0$), (ii) using the Oberbeck-Boussinesq approximation, and finally (iii) specifying constant temperatures boundary conditions (BC) on top-bottom plates, while for the lateral ones we assume perfect insulation conditions. Note that no-slip BC for velocity is taken on every domain boundary. This means that the effects associated to the flow movement in the transverse direction (z axis), or to possible nonlinear buoyancy effects [29], or to the top-bottom asymmetries in the thermal BC which are inevitably present in the experiments [30,31], are all ignored in the calculations. The simulations are performed by means of a multipopulation single-relaxation lattice Boltzmann solver, the same as in Ref. [32]; the computational grids of simulations—which are regular and cartesian—have 512×512 nodes or 1024×1024 nodes for the more demanding cases in spatial

resolution which occur for Ra $= 5 \times 10^8$ at large inclination angles. To obtain statistically converged global quantities each combination of Ra and inclination angle β is simulated for more than 100 large-scale circulation times, $\tau = H/u_{\mathrm{rms}}$ in statistically stationary conditions. The Nusselt number in simulations is computed via Nu $= (\langle u_y T \rangle - \kappa \partial_y \langle T \rangle)/(\kappa \Delta T/H)$, where $\langle \ldots \rangle$ represents an average over time and volume. We will indicate with Nu_t the instantaneous value of the Nusselt number, which is computed by replacing $\langle \ldots \rangle$ by the volume average $\langle \ldots \rangle_V$.

III. FLOW PATTERNS

We begin by characterizing from a qualitative perspective the different flow regimes observed in the CIC system at varying its inclination angle. Two recurrent flow and temperature spatially coherent structures are found in convective cells and particularly in the RBC system: the thermal plumes (TP) and the large-scale circulation (LSC), both of which have significant effects on the global heat transfer in the system [33–35]. The plumes are hot or cold region of the flow that detach in an apparent random fashion from the horizontal thermal boundary layers (BL) and that impinge rapidly into the bulk of the cell under the effect of buoyancy. Their thickness is comparable to the one of the thermal BL but they can lose quickly their coherence under the effect of diffusion or by the turbulent mixing which occurs in the bulk of the cell. The LSC is on the contrary a roll-like flow movement that fills in the full cell producing a wind parallel to all the walls in the system. In the RBC the self-organized LSC has been observed to be either stable or bistable or absent depending on the Pr and Ra values of the system [36–38], while it is always present and oriented in the same direction in the VC [19,22]. We also note that a stronger LSC is known to promote the plume detachment, however the contribution of LSC to the total heat flux with respect to the one of TP is found to be negligible in the RBC for Ra ranging from 10^5 to 10^{11} [39].

In Fig. 2 we report a series of instantaneous visualizations of the flow in the CIC system at different inclination angles and in statistically stationary conditions. In particular we display next to each other snapshots of the velocity and temperature flow field from numerics (panels a–d) and shadowgraph images—whose shading is roughly proportional to the temperature gradient along z—from experiments (panels e–h) at similar inclination angles. The patterns observed appear to be qualitatively similar, supporting therefore the assumption of a quasibidimensional dynamics in our CIC experimental system. In the horizontal case, $\beta = 0$ [Figs. 2(a) and 2(e)], the flow is composed by disordered TP emerging from the boundary layers. The LSC structure is weak, and a single roll can not be clearly identified, this is corroborated by the fact that the plumes, both in the experiment and in the DNS, emerge almost vertically from the BL. A similar flow state, denoted as soft turbulence, has been observed in other high-Pr RBC studies [33,34,40]. Note that the term soft turbulence is used to stress the small scale separation in the flow. Indeed in the RBC, the ratio between the global Kolmogorov scale and the systems size, η/H, can be related exactly to the control parameters $\eta/H = \mathrm{Pr}^{1/2}[\mathrm{Ra}(\mathrm{Nu} - 1)]^{-1/4}$ [41]. It turns out that in our system $\eta/H = 0.1$ at Ra $= 10^8$ and $\eta/H = 0.06$
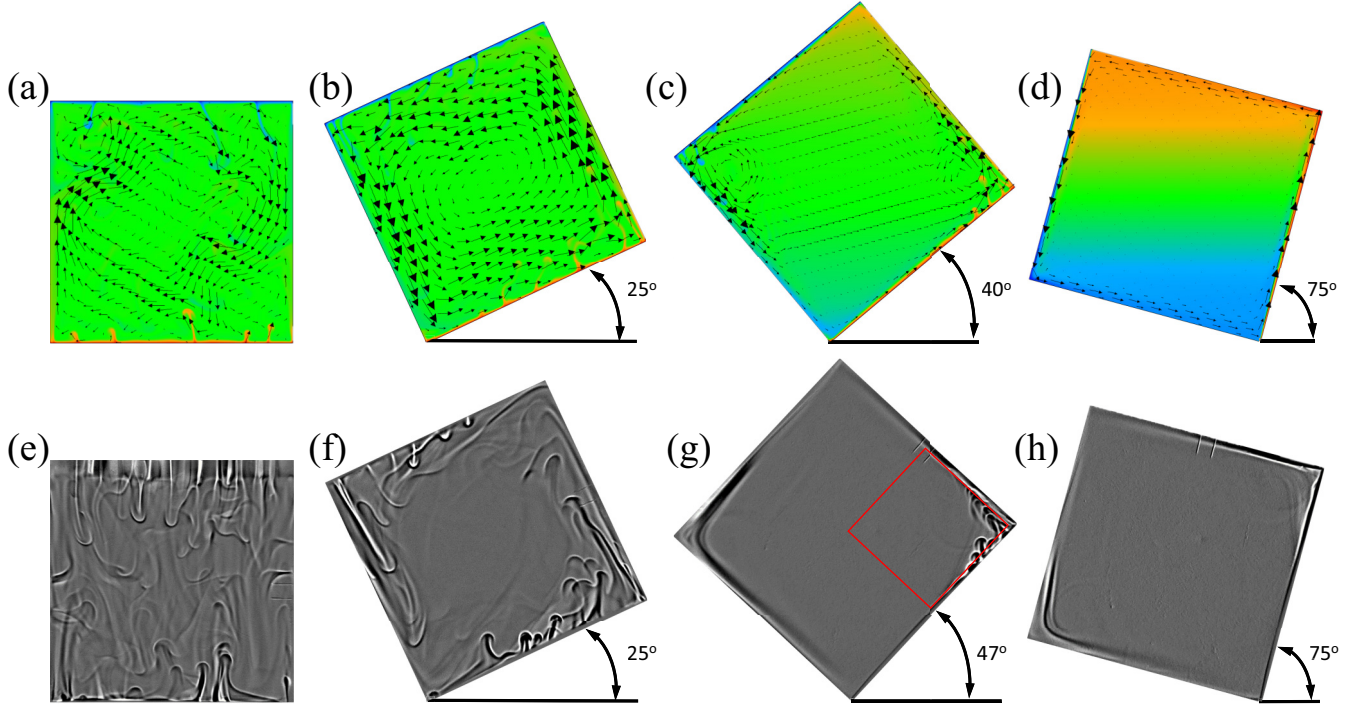
FIG. 2. Visualizations of the instantaneous flow pattern in the CIC cell at Ra $= 5 \times 10^8$ from numerics and experiments for various inclination angles. Panels of the first raw (a)–(d) report visualizations both of the velocity and the temperature field in false colours (red-hot, green-intermediate, blue-cold) for the angles $\beta = 0°$ (a), $\beta = 25°$ (b), $\beta = 40°$ (c), $\beta = 75°$ (d). The second raw (e–h) shows the shadowgraph images of a vertical central plane in the CIC system from the experiments at $\beta = 0°$ (e), $\beta = 25°$ (f), $\beta = 47°$ (g), $\beta = 75°$ (h).

at Ra $= 5 \times 10^8$. For a moderate inclination angle, $\beta = 25°$ [Figs. 2(b) and 2(f)], the LSC appears instead to be well established, the circulation has an elliptical shape at this angle and becomes markedly more space filling and square in shape when β is increased, which is consistent with Ref. [22]. A similar change of LSC shape, from elliptical to square, is also found in the horizontal RBC when Ra (and so Re) is increased [42,43]. At a large inclination angles, $\beta = 75°$ [Figs. 2(d) and 2(h)], the intensity of the velocity results dramatically suppressed. A LSC is still present but any turbulent feature has disappeared, the flow is regular at the boundaries and nearly quiescent in the bulk. As a result the temperature does not display any plume structure and it appears horizontally stratified except for the regimes near to the boundaries, a finding consistent with the numerical results in Ref. [19]. The latter flow state remains nearly unchanged for the $\beta = 90°$ VC case.

A peculiar phenomenon is observed for $\beta \sim 45°$ [Figs. 2(c) and 2(g)], in correspondence to the transition regime from the irregular turbulent-like flow state to the regular one. In such a state, we observe that the TP get generated only on the corners of the cell where the fluid which moves parallel to a hot or cold wall is constrained by the boundary to change direction and, more importantly, the plumes are generated simultaneously in a nearly periodic fashion. This bursting behavior, which to our knowledge as not yet been reported elsewhere, is observed both in experiments and simulations although with a difference: in experiments, due to the asymmetry in the thermal boundary conditions, the plumes do not always detach from the top and bottom boundaries simultaneously (see Supplemental Material [44]

for movies). To better identify the angles at which the bursting phenomenon occurs we investigate, in the DNS, the behavior of the normalized temporal fluctuations of the global velocity intensity, which we define as $I_u = \sigma_t(u_{\rm rms})/\langle u_{\rm rms}\rangle_t$ where $u_{\rm rms}(t) = \sqrt{\langle \mathbf{u} \cdot \mathbf{u} \rangle_V}$ and $\sigma_t(\cdot)$ denotes the temporal standard deviation, and at the same time the fluctuation intensity of heat transfer, $I_{\rm Nu} = \sigma_t({\rm Nu}_t)/{\rm Nu}$, with ${\rm Nu}_t$ the global instantaneous value of the Nusselt number. Both the measurements of $I_u(\beta)$ and $I_{\rm Nu}(\beta)$, reported in Fig. 3, decrease for small inclinations in the turbulent regime and bump-up to the turbulent level in the bursting state, while for larger angles they decrease rapidly to a vanishing value, in support of the observation that the flow becomes laminar and time independent. The inset of Fig. 3 shows the phase diagram of the state of the CIC system in Ra $\times \beta$ space, where we distinguish between the turbulent or chaotic, the bursting and the laminar state, by thresholding over $I_u(\beta)$ (the bursting regime is identified by the criterion $|\partial I_u/\partial \beta| > 1.15$). We find that the bursts occur in a narrow angle range: $\beta \in [32°, 36°]$ at Ra $= 10^8$ and $\beta \in [38°, 42°]$ at Ra $= 5 \times 10^8$. Finally, in Fig. 4 we report the time series for the instantaneous Nusselt number ${\rm Nu}_t$ in DNS for an angle where the system is in the bursting regime. It is evident its oscillatory character with peaks up to 40% higher than the mean. The peaks in Nusselt corresponds to a release of cluster of plumes from the BL into the bulk, proving that in this regime the heat transport by convection is still strongly affected by thermal plumes rather than by the mean flow, in agreement with Ref. [33]. Furthermore it appears that the time-scale associated to the bursts is of the order of $5\tau_\kappa$ where $\tau_\kappa = \lambda_T^2/\kappa$ indicates the thermal diffusion time based on the thermal boundary thickness $\lambda_T = H/(2{\rm Nu})$, see again
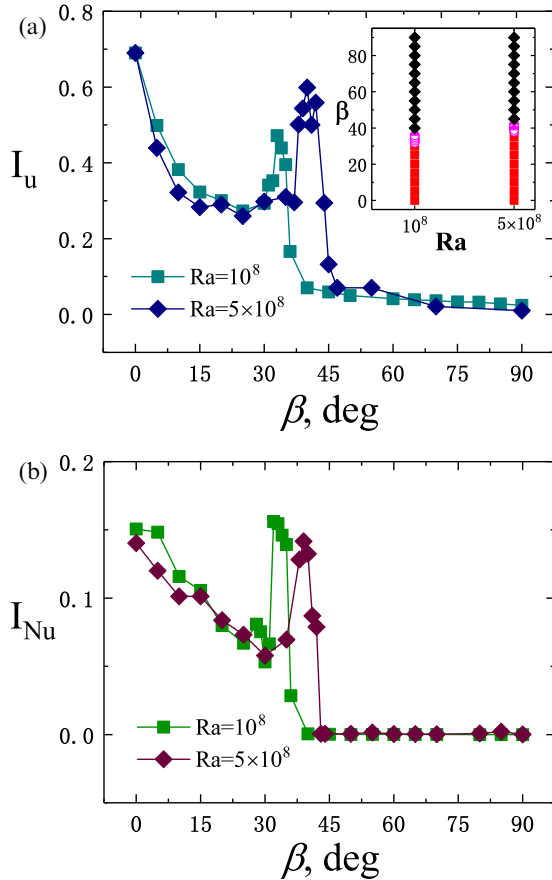
FIG. 3. (a) The fluctuation intensity of the turbulent flow $I_u(\beta)$ in inclined thermal convection for Ra $= 10^8$ (squares) and Ra $= 5 \times 10^8$ (diamonds). Inset: the phase diagram of the flow pattern in the Ra and β plane, the black diamonds refer to the laminar regime, the red squares refer to the turbulent regime and the pink circles refer to the bursting phenomenon regime. (b) The fluctuation intensity of the heat transfer $I_{Nu}(\beta)$ in the inclined thermal convection for Ra $= 10^8$ (squares) and Ra $= 5 \times 10^8$ (diamonds).

Fig. 4. Note however that the observed periodicity is also close to the typical turn over time τ at that inclination, which makes difficult to distinguish the exact physical mechanism for this phenomenon. In the experiments the bursting regime can be highlighted by looking at the time series of the amount of plumes detected in the shadowgraph movies. To identify them we adopt the plumes identification procedure used in Refs. [23,45], which is based on a threshold analysis on the intensity variance of the shadowgraph images, and we then calculate the area fraction of the plumes, A_p appearing in one of the corner of the experiment [inside the red square frame shown in Fig. 2(g)]. Large values of A_p indicates that more plumes are measured in the shadowgraph images. As shown in Fig. 4(b), despite the fact that in the experiments the bursting phenomenon is less regular, it appears to occur with a similar frequency.

IV. HEAT FLUX VARIATION

We now turn the attention on the global and time averaged heat flux in the system, in other words to the Nusselt number
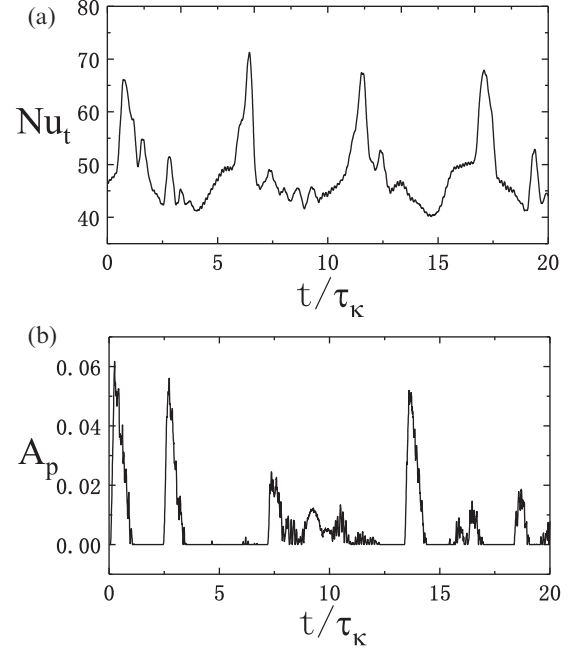

FIG. 4. (a) Time series of instantaneous (volume-averaged) Nusselt number at $\beta = 42°$ for Ra $= 5 \times 10^8$ in simulation. The averaged period of the bursting phenomenon in simulation is about 5τ. (b) Time series of the area fraction of plumes I_p at $\beta = 47°$ for Ra $\simeq 5 \times 10^8$ in experiment. The averaged period of the bursting phenomenon is close to 6τ.

response function. When studying the dependence of Nu(β) it is convenient to take as a reference the Nusselt value measured in the horizontal RBC system Nu(0). In the experiments we measured Nu(0) $\simeq 31.5$ for Ra $\simeq 10^8$ and Nu(0) $\simeq 53.8$ for Ra $\simeq 5 \times 10^8$, which is in agreement with the results obtained in a similar setup at Pr $\simeq 554$, $\Gamma = 1$ [46]. The corresponding values computed from the simulations are Nu(0) $= 29.3 \pm 4.4$ for Ra $= 10^8$ and Nu(0) $= 48.5 \pm 6.9$ for Ra $= 5 \times 10^8$ and are compatible within error bars. Note that in the simulations the statistical error for Nu are estimated from the temporal standard deviations of Nu$_t$ by means of δNu $= \sigma_t(\text{Nu}_t)\sqrt{2\tau_I/\mathcal{T}}$, with τ_I the integral time for Nu$_t$, and $\mathcal{T}$ the total simulation time [47]. On the contrary, in the experiments the positioning of the thermistor inside plates of high thermal inertia prevents from correctly measure the temporal fluctuations of the Nusselt number which turns out to be highly suppressed, as a result a reliable statistical error bar of Nu from experiments could not be evaluated.

Figure 5 shows the normalized Nusselt number Nu(β)/Nu(0) both from experiments and from numerics for the two studied Ra numbers. First, we note the quantitatively similar behavior between experiments and simulations, which is remarkable for the higher-Ra case. Second, we notice that the relative variations of Nu are small: For instance in the DNS the increases of Nu are close to 11.8% for Ra $= 10^8$ and 11.6% for Ra $= 5 \times 10^8$ in the turbulent dominated regime, while in the laminar regime, the enhancements of Nu reaches 19% for Ra $= 10^8$ and 7.4% for Ra $= 5 \times 10^8$. In the experiments the trends are very similar with overall slightly weaker enhancements in the laminar regime as compared
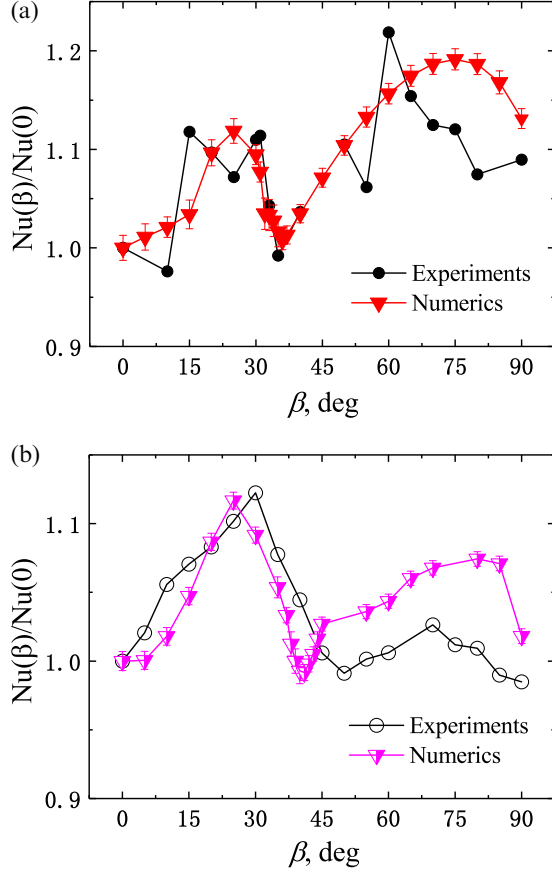
FIG. 5. Nusselt number Nu(β) as a function of the inclination angle β, normalized by its value for $\beta = 0$, from experiments (circles) and numerics (triangles) at (a) Ra $= 10^8$ and (b) Ra $= 5 \times 10^8$. In the experiments the error bars are estimated from $\delta_{\frac{Nu(\beta)}{Nu(0)}} = \frac{Nu(\beta)}{Nu(0)} \sqrt{\left[\frac{\delta Nu(\beta)}{Nu(\beta)}\right]^2 + \left[\frac{\delta Nu(0)}{Nu(0)}\right]^2}$.

to DNS. The little variations of Nu as a function of the inclination angle is a remarkable effect if one considers that at varying the angle the nature of the flow changes from a turbulent and plume dominated one to a time independent laminar flow and it attests for what we denote as robustness of the heat transfer convective process in this type of system. Looking more in detail on the Nu(β) trend one can observe a "bimodal" dependence, characterized by the presence of two local-maxima. For Ra $= 10^8$ in simulations, the Nu increases in the turbulent dominated regime to a local maximum at $\beta \sim 25°$ and descends to a minimum point at $\beta = 36°$ in the bursting flow regime. For higher angles Nu increases again to a second maximum at $\beta \sim 75°$ and drops a little for 90°. For Ra $= 10^8$ in experiments, the bimodal trend is less distinct, but the agreement on Nu amplitude is clear in the bursting regime. The curves of Nu(β)/Nu(0) for Ra $= 5 \times 10^8$ have a similar trend although with a tiny shift towards larger angles for the local minima corresponding to an angle shift in the bursting regime.

We remark that these results are significantly different from the ones of previous experiments in the same cell geometry at smaller Prandtl number Pr $\simeq 6.3$, Ra $\sim 10^9$ [22] and Pr $\simeq 10$, Ra $\sim 10^{10}$ [23] in which Nu monotonously decreases by

20% by increasing β. Instead a qualitatively similar double-peaked variation of Nu is found in DNS in a cylinder of aspect ratio 1 at Pr $= 10$ and Pr $= 100$, Ra $= 10^7$ [19]. The same numerical study shows that the behavior of Nu(β) at changing Pr for fixed Ra evolves from the one with single-peak to one with two peaks. This points to the fact that the magnitude of Pr may be of key importance in this respect.

V. REYNOLDS NUMBER VARIATION

To complement our findings on the heat flux we investigate the variation of the response function given by the Reynolds number at varying the inclination angle. As mentioned before, one way to define the Reynolds number is by means of the global root-mean-squared (rms) velocity, $u_{\text{rms}} = \sqrt{\langle \mathbf{u} \cdot \mathbf{u} \rangle}$, so Re $= u_{\text{rms}} H / \nu$; however, in the simulations, where the full velocity field is available, it is convenient to consider also Reynolds number based on the single rms components of the velocities, i.e., Re$_x$ and Re$_y$. On the contrary, in the experiment the measurement of the velocity field is only performed locally by analyzing the cross correlation signal from a couple of thermistors positioned next to an insulating wall in the cell. Such a method works only when the mean flow is robust [28] (see also Refs. [48,49] for its application in the RBC system), and in conclusion it may be applied only when a vigorous LSC is present in the system. This limitation prevented us from measuring the velocity field for every inclination, and made it possible to have a reliable Reynolds estimate, denoted Re$_l = U_y H / \nu$ (where U_y denotes the local y direction rms velocity estimated by elliptic model [28]), only for the higher Ra number experiment. All the described Reynolds number measurements are reported as a function of the tilting angle β in the main panels of Figs. 6(a) and 6(b). Their intensity if we compare the two Ra varies of about a factor $\sqrt{5}$ in a agreement with the approximate scaling law Re $\sim$ Ra$^{1/2}$ [12], which is larger than the variation detected in the amplitude of Nu (which scales roughly as $\sim$Ra$^{1/3}$ or $\sim$ Ra$^{1/4}$). Also note that the magnitude of Re for $\beta = 0°$ is much smaller than one observed in RBC at small Pr [20]. For what concerns the β dependency, we observe that in the turbulence dominated regime all the curves increase to a maximum corresponding to a weak tilting at $\beta \simeq 10°$ and then they drop rapidly till a value Re ~ 2 for angles which correspond roughly to the occurrence of a local minimum in the Nu(β) (see again of Fig. 5). Finally, for larger angles the decrease in Re is much more gentle and reaches values which correspond to a creeping flow. In Fig. 6(b) we see that the single peak behavior for Re(β) is also supported by the measurements of Re$_l$ from the experiment, which are in good agreement with the numerical value of Re$_{x,y}$. Notice however that the Re$_l$ at large β could not be estimated in the experiments for the laminar regime due to the extreme weakness of the flow. Let us remark that the curves of Re is again different from the experimental results at smaller Prandtl number, where it is generally observed a peak occurring also at $\beta \simeq 10 \pm 2°$ but followed by a linear decrease till the largest inclinations [19,22,23].

To better appreciate the link between the behaviours of Re and Nu at varying the inclination we plot, in the insets of Fig. 6, their normalized trends with respect to the flat cell case. First let us observe that the overall variations of
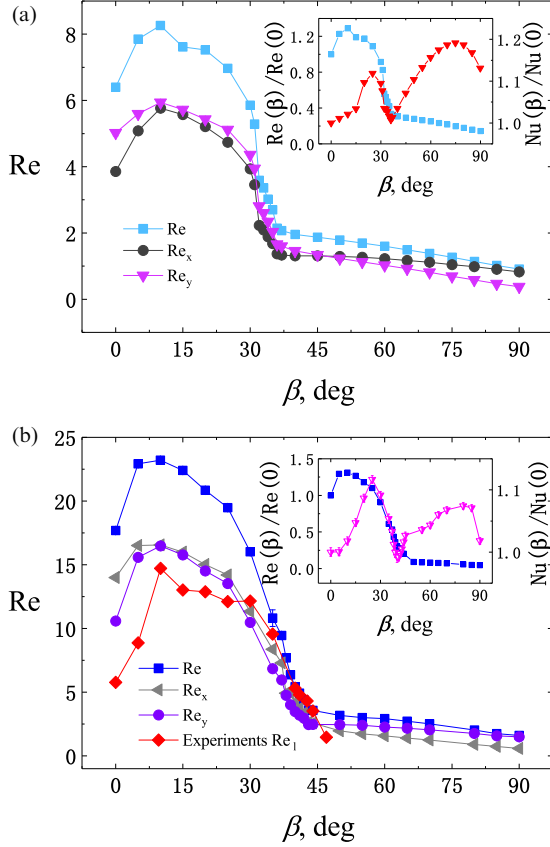
FIG. 6. Reynolds numbers as functions of the inclination angle β: (a) for Ra $= 10^8$. (b) for Ra $= 5 \times 10^8$. In (b) we report also the local Reynolds number Re$_l$ from experiments is (red diamonds). In the insets: the superposed graphs for Re(β)/Re(0) (squares) and Nu(β)/Nu(0) (triangles) from DNS.

Re(β)/Re(0) are of more than 85%, much more pronounced than for Nu(β)/Nu(0). Furthermore, in the turbulent regime even if the peaks in Re and Nu are not coincident it appears that after such maxima there is an evident correlation between the sharp decrease of both these observables. In the laminar regime however, such correlation is lost and the robustness of the heat-flux seems therefore not connected to fluctuations of the velocity.

The noncoincidence of the peaks in Re(β) and Nu(β) may be due to the fact that the definition of the Re based on the rms velocity does not reliably account for the the intensity of the LSC. To properly quantify the intensity of the LSC, rather than measuring the velocity fluctuations one should extract the amplitude of the mean flow in the system. To this aim we apply to the numerical data a technique proposed in Ref. [47], based on conditional average of the flow field with respect to the sign of the vorticity, ω, in a point at the center of the system which allows to compute both time averaged velocity flow patterns $\overline{u}_x(x, y) = \langle u_x \text{sign}(\omega) \rangle_t$ and $\overline{u}_y(x, y) = \langle u_y \text{sign}(\omega) \rangle_t$. In Fig. 7 we show the average spatial profiles of these conditional fields, i.e., $U_x(y) \equiv \langle \overline{u}_x \rangle_{x(y)}$ and $U_y(x) \equiv \langle \overline{u}_y \rangle_{y(x)}$, computed over a time history of about 20 τ and where $\langle \ldots \rangle_{x(y)}$ and $\langle \ldots \rangle_{y(x)}$ represent the line averaging along the x direction for fixed y or along the y direction for fixed x. We remark that the vertical velocity profile associated to the LSC structure,
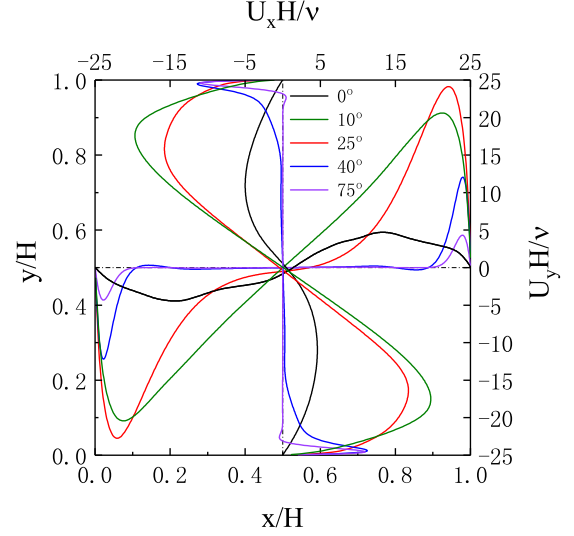

FIG. 7. The vertical $U_y(x)$ and horizontal $U_x(y)$ velocity profiles associated to the LSC flow structure as derived from the conditionally time averaged velocity fields $\overline{u}_x$ and $\overline{u}_y$ at different inclination angles for Ra $= 5 \times 10^8$. The abscissa and ordinate scales are the dimensionless width and height. The upper scales show the horizontal velocity profiles nondimensionalized with ν/H, i.e., Re$_x(y)$; the right scales show the vertical velocity's $U_y(x)$ profiles, also nondimensionalized by ν/H.

$U_y(x)$, reaches a maximum for the inclination angle $\beta = 25°$. This coincide with the angle for which the first peak in Nu(β) is observed in the same conditions (same Ra). Because the y component of the velocity enters into the definition of the Nu number this observation supports the hypothesis that the first peak of Nu(β)/Nu(0) is due to an enhancement of the LSC intensity (and specifically the enhancement of its y axis component). From Fig. 7 we also see that a LSC is still present in the laminar regime; however, it decreases by increasing β and becomes progressively more attached to the walls (one expects indeed that the thickness of a laminar boundary layer will be proportional to Re$_{x,y}^{1/2}$). It is not possible in this case to correlate the Re(β) trend with the second peak observed in Nu(β).

VI. HEAT-FLUX AND COHERENT FLOW STRUCTURES

The fact that the intensity of the heat flux remains high even in the laminar regime where the mean flow is progressively weakening and the temporal fluctuations are absent is a puzzling effect. To make sense on this phenomenon it is useful to look at the time-averaged global correlation coefficient of the velocity component in the direction of the imposed thermal gradient, u_y, with the temperature field itself, which is defined as

$$C_{u_y T} = \left\langle \frac{\langle u_y' T' \rangle_V}{\sqrt{\langle u_y'^2 \rangle_V \langle T'^2 \rangle_V}} \right\rangle_t, \qquad (1)$$

where $u_y' = u_y - \langle u_y \rangle_V$ and $T' = T - \langle T \rangle_V$ denote the deviation from the mean; note, however, that $\langle u_y \rangle_V = 0$ because the system is bounded and $\langle T \rangle_V = (T_{\text{hot}} + T_{\text{cold}})/2$ the arithmetic mean of the plates temperatures. The function
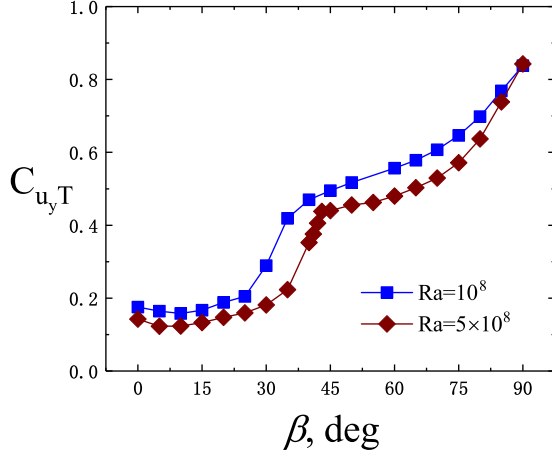
FIG. 8. Correlation coefficient of y-axis velocity u_y and temperature T, $C_{u_y T}$, in inclined convection as a function of inclination angle β for Ra $= 10^8$ (squares) and Ra $= 5 \times 10^8$ (diamonds).

$C_{u_y T}(\beta)$ represents the efficiency of the flow in transporting the heat across the cell, and it is shown in Fig. 8 for both Ra of the numerical study. In the turbulent dominated regime, $C_{u_y T}$ is small because the only regions where the velocity and temperature fields are correlated is in the TP, which are destroyed by the turbulent fluctuations of the bulk, and so they occupy a small fraction of the whole system; furthermore, the overall velocity intensity which is in the denominator is large as so the resulting overall correlation is small. In the bursting regime, $C_{u_y T}$ begins to increase rapidly, this due to the decrease of the velocity intensity, and finally becomes very large in the laminar regime, indicating that the residual slow motion of fluid becomes more effective in transporting heat. Remarkably, for the largest inclination which corresponds to the VC system the correlation is as high as 85%.

Such an analysis can be further refined by quantifying the amount of heat Nu$_c$ which is transported through the coherent structures. The method we adopt here was first proposed for the RBC system to identify the plumes in a convective flow [50–52]. This method is based on a thresholding procedure both on the instantaneous correlation field of u_y with T and on the instantaneous intensity of the temperature itself (in accordance with Ref. [51], the empirical thresholding constant on the correlation c is chosen to be 1.2). The resulting visualizations (not shown here) identify as coherent flow regions mostly the TP in the turbulent regime and the thin LSC roll in the laminar one. Though the magnitude of Nu$_c(\beta)/$Nu(0) slightly depends on the criterion of detection of coherent structure, it is clear from Fig. 9 that there exist a strong correlation between Nu$(\beta)/$Nu(0) and Nu$_c(\beta)/$Nu(0) only in the laminar regime. Therefore, it appears even more clearly that the large heat flow observed for large inclinations (laminar regime) is due to the strong correlation of temperature and velocity in the LSC region of the flow. While, on the contrary, in the turbulent regime such an identification between flow structures (LSC or TP) and heat transport is much more complex, or at least not detectable with this analytical tool. Note that the value of the Pr number plays a crucial role here. Indeed the time it takes for a patch to be spread by diffusion with respect to the time it takes to be transported by a flow
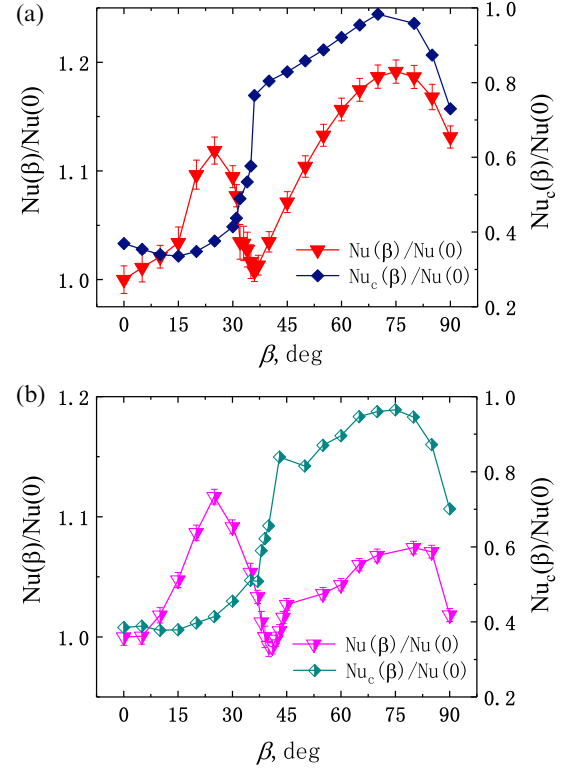

FIG. 9. Normalized Nusselt number Nu$(\beta)/$Nu(0) (triangles) and fraction of heat transfer, Nu$_c(\beta)/$Nu(0), carried by the coherent structure (diamonds) for (a) Ra $= 10^8$ and (b) Ra $= 5 \times 10^8$ as functions of the inclination angle β.

of given intensity is given by the Péclet (Pe) number that is Pe $=$ Re Pr. This means that even when the flow is in creeping conditions, take, e.g., Re ~ 0.2 the convective time is $O(10^2)$ shorter than the diffusion one (Pe ~ 100). This might offer a key on why such a trend for Nu(β) in the laminar regime was not observed in any of the studies at lower Pr.

VII. CONCLUSIONS

In this paper, we have investigated the behavior of confined inclined convection in a quasibidimensional rectangular system of unit aspect ratio at a constant Prandtl number, Pr $\simeq 480$, and Rayleigh numbers (Ra $= 10^8$ and 5×10^8) by means of experiments and simulations. In particular we have focused on the characterization of the flow patterns and on the key response functions Nu and Re with respect to the inclination angle. By progressively tilting the system from $\beta = 0°$ to $\beta = 90°$ the flow changed from a soft-turbulent state, dominated by plumes which penetrate well into the bulk of the system and that perturb considerably the LSC, to a steady laminar state where a LSC steady coherent structure is markedly dominant and plumes are absent. Based on the analysis of flow patterns at changing the inclination angle, we classified the system behavior into three regimes: (i) turbulent, (ii) bursting, and (iii) laminar. Despite the major differences observed in the flow organization, the measured variations of Nu are only less than 20% at Ra $= 10^8$ and 10% at Ra $= 5 \times 10^8$, while the variations of Re are larger than 85% in all cases. More specifically, the Nusselt number

shows a nonmonotonic two-peak dependency on varying the inclination angle. Such a feature is clearly confirmed both in simulations and in the experiments. The $Re(\beta)$ instead has a single peak occurring at relatively small angles $\sim 10°$ followed by a sharp decrease and a near flat behavior for large inclinations. In the turbulent regime, it is found that the first peak of $Nu(\beta)/Nu(0)$ is due to the enhancement of the LSC, specifically the enhancement of its component in the direction of the imposed thermal gradient (y component). The dependence of Nu and Re on large inclinations found in our study is very different in comparison to previous studies conducted in a comparable range of Ra values, in identical containers [22,23] (or containers with similar aspect ratio [19]) but with rather different Pr values. In the light of this we advance the hypothesis that the high heat-flux observed in our setup in the laminar regime depends primarily the high-Pr value. In such a condition indeed the temperature diffuses much less than the velocity and it is enslaved to the flow structure and therefore efficiently transported by the laminar LSC; in dimensionless terms the characteristic Péclet number of the flow is here always much larger than one, a condition which is not encountered in the previous mentioned studies.

In summary this study tells that the global heat transfer of thermal convection in a cell with the present features, i.e., $\Gamma = 1$, $Pr \gg 1$, $Ra \simeq 10^8$, and $Ra \simeq 5 \times 10^8$ is robust and is not sensitive to the cessation of turbulence. Furthermore, the laminar heat transfer state is not only equally efficient but it is also steady, while the turbulent one fluctuates vigorously in time. Our results contradict the common wisdom that turbulent thermal convection can be much more efficient in transferring heat than a laminar flow and, in this respect, are in agreement with previous studies at $\Gamma = 1$ in different conditions. The present study also confirms the complex character of the CIC dynamics, which deserves to be explored in its full parameter space in forthcoming studies.

[1] B. Castaing, G. Gunaratne, F. Heslot, L. Kadanoff, A. Libchaber, S. Thomae, X. Wu, S. Zaleski, and G. Zanetti, J. Fluid Mech. **204**, 1 (1989).

[2] E. Siggia, Annu. Rev. Fluid Mech. **26**, 137 (1994).

[3] G. Ahlers, S. Grossmann, and D. Lohse, Rev. Mod. Phys. **81**, 503 (2009).

[4] D. Lohse and K.-Q. Xia, Annu. Rev. Fluid Mech. **42**, 335 (2010).

[5] F. Chillà and J. Schumacher, Eur. Phys. J. E **35**, 58 (2012).

[6] A. Bejan and C. L. Tien, J. Heat Transfer **100**, 641 (1978).

[7] H. Yu, N. Li, and R. E. Ecke, Phys. Rev. E **76**, 026303 (2007).

[8] J. Patterson and J. Imberger, J. Fluid Mech. **100**, 65 (1980).

[9] O. Shishkina, Phys. Rev. E **93**, 051102 (2016).

[10] C. S. Ng, A. Ooi, D. Lohse, and D. Chung, J. Fluid Mech. **764**, 349 (2015).

[11] S. Grossmann and D. Lohse, Phys. Rev. Lett. **86**, 3316 (2001).

[12] S. Grossmann and D. Lohse, J. Fluid Mech. **407**, 27 (2000).

[13] R. J. A. M. Stevens, D. Lohse, and R. Verzicco, J. Fluid Mech. **688**, 31 (2011).

[14] S. W. Churchill and H. H. S. Chu, Int. J. Heat Mass Transf. **18**, 1323 (1975).

[15] T. Tsuji and Y. Nagano, Int. J. Heat Mass Transf. **31**, 1723 (1988).

[16] T. A. M. Versteegh and F. T. M. Nieuwstadt, Int. J. Heat Mass Transf. **42**, 3673 (1999).

[17] P. Kiš and H. Herwig, Int. J. Heat Mass Transf. **55**, 2625 (2012).

[18] W. K. George and S. P. Capp, Int. J. Heat Mass Transf. **22**, 813 (1979).

[19] O. Shishkina and S. Horn, J. Fluid Mech. **790**, R3 (2016).

[20] L. Zwirner and O. Shishkina, J. Fluid Mech. **850**, 984 (2018).

[21] J. N. Arnold, I. Catton, and D. K. Edwards, J. Heat Transfer **98**, 67 (1976).

[22] S.-X. Guo, S.-Q. Zhou, X.-R. Cen, L. Qu, Y.-Z. Lu, L. Sun, and X.-D. Shang, J. Fluid Mech. **762**, 273 (2014).

[23] S. X. Guo, S. Q. Zhou, L. Qu, X. R. Cen, and Y. Z. Lu, Int. J. Heat Mass Transf. **111**, 933 (2017).

[24] R. Khalilov, I. Kolesnichenko, A. Pavlinov, A. Mamykin, A. Shestakov, and P. Frick, Phys. Rev. Fluids **3**, 043503 (2018).

[25] A. Vasil'ev, I. Kolesnichenko, A. Mamykin, P. Frick, R. Khalilov, S. Rogozhkin, and V. Pakholkov, Tech. Phys. **60**, 1305 (2015).

[26] A. Baïri, N. Laraqi, and J. M. García de María, Exp. Thermal Fluid Sci. **31**, 309 (2007).

[27] J. S. Steinhart and S. R. Hart, Deep Sea Res. Ocean. Abs. **15**, 497 (1968).

[28] G.-W. He and J.-B. Zhang, Phys. Rev. E **73**, 055303 (2006).

[29] G. Ahlers, E. Calzavarini, F. F. Araujo, D. Funfschilling, S. Grossmann, D. Lohse, and K. Sugiyama, Phys. Rev. E **77**, 046302 (2008).

[30] S.-D. Huang, F. Wang, H.-D. Xi, and K.-Q. Xia, Phys. Rev. Lett. **115**, 154502 (2015).

[31] H. Johnston and C. R. Doering, Phys. Rev. Lett. **102**, 064501 (2009).

[32] K. Shrestha, G. Mompean, and E. Calzavarini, Phys. Rev. E **93**, 023306 (2016).

[33] X.-D. Shang, X.-L. Qiu, P. Tong, and K.-Q. Xia, Phys. Rev. Lett. **90**, 074501 (2003).

[34] X.-D. Shang, X.-L. Qiu, P. Tong, and K.-Q. Xia, Phys. Rev. E **70**, 026308 (2004).

[35] D. Funfschilling and G. Ahlers, Phys. Rev. Lett. **92**, 194502 (2004).

[36] E. Brown and G. Ahlers, J. Fluid Mech. **568**, 351 (2006).

[37] K. Sugiyama, R. Ni, R. J. A. M. Stevens, T. S. Chan, S.-Q. Zhou, H.-D. Xi, C. Sun, S. Grossmann, K.-Q. Xia, and D. Lohse, Phys. Rev. Lett. **105**, 034503 (2010).

[38] F. F. Araujo, S. Grossmann, and D. Lohse, Phys. Rev. Lett. **95**, 084502 (2005).

[39] A. Belmonte, A. Tilgner, and A. Libchaber, Phys. Rev. Lett. **70**, 4067 (1993).

[40] H.-D. Xi, S.-Q. Zhou, Q. Zhou, T.-S. Chan, and K.-Q. Xia, Phys. Rev. Lett. **102**, 044503 (2009).

[41] K. Sugiyama, E. Calzavarini, S. Grossmann, and D. Lohse, Europhys. Lett. **80**, 34002 (2007).

[42] J. J. Niemela and K. R. Sreenivasan, Europhys. Lett. **62**, 829 (2003).

[43] K.-Q. Xia, C. Sun, and S.-Q. Zhou, Phys. Rev. E **68**, 066303 (2003).

[44] See Supplemental Material at http://link.aps.org/supplemental/10.1103/PhysRevE.99.013108 for movies of the plume bursting phenomenon.

[45] S.-Q. Zhou, N. Eber, A. Buka, W. Pesch, and G. Ahlers, Phys. Rev. E **74**, 046211 (2006).

[46] K.-Q. Xia, S. Lam, and S. Q. Zhou, Phys. Rev. Lett. **88**, 064501 (2002).

[47] K. Sugiyama, E. Calzavarini, S. Grossmann, and D. Lohse, J. Fluid Mech. **637**, 105 (2009).

[48] X. He, D. P. M. Van Gils, E. Bodenschatz, and G. Ahlers, New J. Phys. **17**, 063028 (2015).

[49] Q. Zhou, C.-M. Li, Z.-M. Lu, and Y.-L. Liu, J. Fluid Mech. **683**, 94 (2011).

[50] E. S. C. Ching, H. Guo, X.-D. Shang, P. Tong, and K.-Q. Xia, Phys. Rev. Lett. **93**, 124501 (2004).

[51] E. Van der Poel, R. Verzicco, S. Grossmann, and D. Lohse, J. Fluid Mech. **772**, 5 (2015).

[52] S. D. Huang, M. Kaczorowski, R. Ni, and K.-Q. Xia, Phys. Rev. Lett. **111**, 104501 (2013).